Regulation of the NMDA Component of EPSPs by Different Components of Postsynaptic GABAergic Inhibition: Computer Simulation Analysis in Piriform Cortex

A. KAPUR,[1] W. W. LYTTON,[1,2] K. L. KETCHUM,[3] AND L. B. HABERLY[1,3]
[1]*Neuroscience Program,* [2]*Department of Neurology, and* [3]*Department of Anatomy, University of Wisconsin, Madison, Wisconsin 53706*

Kapur, A., W. W. Lytton, K. L. Ketchum, and L. B. Haberly. Regulation of the NMDA component of EPSPs by different components of postsynaptic GABAergic inhibition: computer simulation analysis in piriform cortex. *J. Neurophysiol.* 78: 2546–2559, 1997. Physiological analysis in the companion paper demonstrated that γ-aminobutyric acid-A ($GABA_A$)-mediated inhibition in piriform cortex is generated by circuits that are largely independent in apical dendritic and somatic regions of pyramidal cells and that $GABA_A$-mediated inhibitory postsynaptic currents (IPSCs) in distal dendrites have a slower time course than those in the somatic region. This study used modeling methods to explore these characteristics of $GABA_A$-mediated inhibition with respect to regulation of the *N*-methyl-D-aspartate (NMDA) component of excitatory postsynaptic potentials. Such regulation is relevant to understanding NMDA-dependent long-term potentiation (LTP) and the integration of repetitive synaptic inputs that can activate the NMDA component as well as pathological processes that can be activated by overexpression of the NMDA component. A working hypothesis was that the independence and differing properties of IPSCs in apical dendritic and somatic regions provide a means whereby the NMDA component and other dendritic processes can be controlled by way of GABAergic tone without substantially altering system excitability. The analysis was performed on a branched compartmental model of a pyramidal cell in piriform cortex constructed with physiological and anatomic data derived by whole cell patch recording. Simulations with the model revealed that NMDA expression is more effectively blocked by the slow $GABA_A$ component than the fast. Because the slow component is present in greater proportion in apical dendritic than somatic regions, this characteristic would increase the capacity of dendritic IPSCs to regulate NMDA-mediated processes. The simulations further revealed that somatic-region GABAergic inhibition can regulate the generation of action potentials with little effect on the NMDA component generated by afferent fibers in apical dendrites. As a result, if expression of the NMDA component or other dendritic processes were enabled by selective block of dendritic inhibition, for example, by centrifugal fiber systems that may regulate learning and memory, the somatic-region IPSC could preserve system stability through feedback regulation of firing without counteracting the effect of the dendritic-region block. Simulations with paired inputs revealed that the dendritic $GABA_A$-mediated IPSC can regulate the extent to which a strong excitatory input facilitates the NMDA component of a concurrent weak input, providing a possible mechanism for control of ''associative LTP'' that has been demonstrated in this system. Postsynaptic $GABA_B$-mediated inhibition had less effect on the NMDA component than either the fast or slow $GABA_A$ components. Depolarization from a concomitant α-amino-3-hydroxy-5-methyl-4-isoxazolepropionic acid (AMPA) component also was found to have comparatively little effect on current through the NMDA channel because of its brief time course.

INTRODUCTION

The companion paper provided evidence for piriform cortex that γ-aminobutyric acid-A ($GABA_A$)-mediated inhibitory postsynaptic currents (IPSCs) are generated in apical dendrites as well as cell bodies, that the neuronal circuitry that generates IPSCs in distal dendritic and somatic regions is largely separate, that $GABA_A$ inhibition consists of fast and slow components, and that there is a greater proportion of the slow component in distal dendrites than cell bodies (Kapur et al. 1997). Other studies in piriform cortex have demonstrated that $GABA_B$-mediated IPSCs also are generated in pyramidal cell dendrites (Kanter et al. 1996; Tseng and Haberly 1988).

There is now evidence for piriform cortex (Kanter et al. 1996), as originally demonstrated in other cortical areas (Dingledine et al. 1986; Garthwaite and Garthwaite 1989; Luhmann and Prince 1990), that the NMDA component of EPSCs is blocked readily by GABAergic inhibition. In piriform cortex, selective blockade of dendritic $GABA_A$ inhibition enables expression of the NMDA component in response to burst stimulation (Kanter et al. 1996). This raises the possibility that the modulation of NMDA-dependent LTP by $GABA_A$ inhibition that has been demonstrated in piriform cortex (del Cerro et al. 1992; Kanter and Haberly 1993) and other cortical areas (Artola et al. 1990; Steward et al. 1990; Tomasulo et al. 1993; Zhang and Levy 1993) is exerted, at least in part, by direct action on the NMDA component. GABAergic regulation of current through NMDA channels and the resulting voltage changes also may have functional consequences for integrative processes as well as pathological processes that can result from excessive current through NMDA channels or regenerative bursting.

This study uses modeling methods to explore the capacity of different components of GABAergic inhibition to regulate the NMDA component through its voltage-dependent conductance. Much of this analysis was guided by the working hypothesis that the independence and differing properties of IPSCs in dendritic and somatic regions allow NMDA-mediated processes to be controlled without substantially altering system excitability. The slower decay of the dendritic $GABA_A$-mediated IPSC could increase its capacity to control the NMDA component, which it resembles in time course. If this IPSC is suppressed selectively, as, for example, by centrifugal fibers that might regulate learning and memory, the resulting increase in system excitability would

be lessened. The increase in excitability that does occur would elicit an increase in the feedback somatic-region IPSC thereby maintaining excitability in the optimal range. By virtue of its location and faster time course, the somatic-region IPSC could regulate output (firing) while having minimal effect on the NMDA component that is generated exclusively in the dendrites of pyramidal cells.

Modeling methods were used to test two key predictions from this hypothesis: that the slow component of the $GABA_A$-mediated IPSC is optimal for regulating the NMDA component, and that the somatic IPSC can regulate effectively the generation of action potentials with little effect on the NMDA component. Related issues that were investigated included the ability of $GABA_B$-mediated inhibition to regulate the NMDA component, effects of a concomitant α-amino-3-hydroxy-5-methyl-4-isoxazolepropionic acid (AMPA) component on current through NMDA channels, and GABAergic regulation of the extent to which strong excitatory inputs facilitate the NMDA component of concurrent weak inputs—an issue regarding the mechanism of ''associative LTP'' (Gustafsson and Wigstrom 1986; Kanter and Haberly 1993; Tomasulo et al. 1993; Zhang and Levy 1993).

The analysis was carried out on a fully branched compartmental model of a superficial pyramidal cell in piriform cortex that was constructed with physiological and anatomic data derived by whole cell patch recording. As demonstrated in recent studies in other systems (Jonas et al. 1993; Major et al. 1994; Thurbon et al. 1994), the use of whole cell patch recording to derive physiological parameters allowed voltage transients to be simulated accurately without the need for the introduction of a somatic shunt. Cable parameters were determined using the method of Holmes and Rall (1992).

The results showed that cable parameters for pyramidal cells in piriform cortex are comparable with those in the CA1 region of hippocampus, that inhibition mediated by the slow $GABA_A$ conductance component is more effective than the fast $GABA_A$ component or $GABA_B$ inhibition for regulating the NMDA component, and that somatic inhibition of sufficient strength to control the generation of action potentials has little or no effect on the NMDA component evoked by repetitive stimulation of afferent fibers.

METHODS

Physiological measurements

Physiological data were derived from voltage responses to current pulses injected at the soma using the blind, whole cell patch technique (Blanton et al. 1989). Recordings were made in 0.5-mm-thick slices of piriform cortex obtained from 4-wk-old male Sprague Dawley rats. Slices were cut perpendicular to the cortical surface with a Vibratome (Lancer) in oxygen-saturated medium at ~4°C. The medium for slicing and recording contained (in mM) 126 NaCl, 3 KCl, 2 $CaCl_2$, 1 $MgSO_4$, 1.25 NaH_2PO_4, 26 $NaHCO_3$, and 10 D-glucose, equilibrated with 95% O_2-5% CO_2. Recordings were obtained from submerged slices at 29°C, using the chamber described by Tseng and Haberly (1988). Recording pipettes contained (in mM) 130 K-gluconate, 5 KCl, 2 $MgCl_2$, 0.5 $CaCl_2$, 10 *N*-[2-hydroxyethyl] piperazine-*N*′-[2-ethanesulfonic acid] (HEPES, sodium salt), 5 ethylene glycol-bis(β-aminoethylether) *N*,*N*,*N*′,*N*′-tetraacetic acid (EGTA), 2 adenosine 5′-triphosphate (ATP, Mg salt), and 1% Neurobiotin (Vector Labs). The solution was buffered with KOH to pH 7.3; final osmolarity was 290–330 mOsm. Pipette resistance, measured extracellularly, was 7–12 MΩ. Recordings were made with an Axoclamp 2A amplifier (Axon Instruments) in bridge mode.

Input resistance, R_N, the membrane time constant, τ_0, and the coefficient of the membrane time constant, C_0, were determined from voltage responses to current pulses delivered at the soma. Low amplitude (0.01–0.02 nA) hyperpolarizing current pulses were used for this purpose to minimize activation of voltage-gated conductances. R_N was calculated from the steady state amplitude of the voltage response; τ_0 and C_0 were obtained by fitting voltage transients generated by the onset and/or offset of the current pulse with a biexponential function, using the simplex routine provided in pClamp V5.5 (Axon Instruments).

Morphological measurements

Superficial pyramidal cells were stained by diffusion of Neurobiotin from the patch pipettes. Slices were fixed by submersion in 4% formaldehyde (prepared from paraformaldehyde) in phosphate buffer at pH 7.4, cryoprotected in 20% sucrose and 10% glycerol in phosphate buffer, and serially sectioned at 60 μm thickness after flattening in the plane of the microtome knife during freezing with light pressure from a glass slide. Neurobiotin was visualized with the avidin-biotin reaction using the Standard ABC kit from Vector Labs, with Co^{2+} and Ni^{2+}-intensified 2,2′ diaminobenzidine as the chromagen (Adams 1977, 1981). Sections were dried onto subbed slides, lightly counterstained with cresyl violet to visualize cortical layers, and dehydrated and cleared with conventional methods.

The three-dimensional structure of neurons was reconstructed from serial sections with the Eutectic Neuron Tracing System. Distances in the *z* dimension (thickness) were corrected for shrinkage (order of 10-fold). The shrinkage factor was determined separately for each section based on the original thickness and the actual thickness after histological processing. There was little shrinkage in the plane of sections because of the attachment to subbed slides.

The total area of membrane on dendritic spines was computed from estimates of numbers and dimensions of spines. Twenty dendritic segments (branch point to subsequent branch point or termination) were selected at random from one of the reconstructed cells (*40C2*), and the number of spines on each segment counted using a ×100 objective in blue light (n = 606). Because most spines on layer II pyramidal cells in piriform cortex are on dendrites that are <1.5 μm in diameter and spines that were above dendritic shafts could be visualized readily, no correction factor for obscured spines was made. Based on these counts, approximations were made for the density of spines per unit membrane area as a function of distance from cell bodies, from which total numbers could be derived from compartmental dimensions. Diameters of spine heads were estimated with a camera lucida by overlaying spines with dots of known diameters, again at ×100 in blue light (n = 278). Average spine neck diameter was estimated from measurements on electron micrographs.

Simulation methods

The analysis of interactions between inhibitory and excitatory conductances was carried out by inserting simulated synaptic conductances at the appropriate locations in a detailed compartmental representation of a pyramidal cell in piriform cortex. The procedures used for determining membrane resistivity (R_m), membrane capacitance (C_m), and cytoplasmic resistivity (R_i) are described in APPENDIX A. The simulations were performed on a Sun SPARC station using Neuron (Hines 1989). A time step of 0.25 ms was used throughout. Tests with a time step of 0.05 ms confirmed that the time course of IPSCs was not altered by the use of a 0.25-ms step.

Excitatory synaptic action was simulated by modeling AMPA and NMDA conductances. Inhibitory synaptic inputs included the

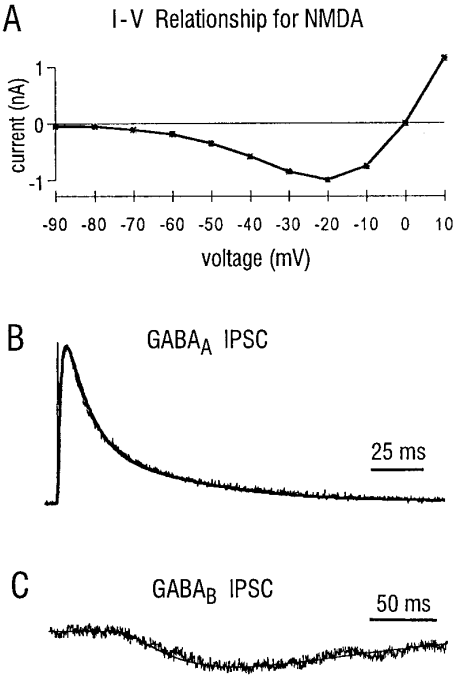

FIG. 1. Model synaptic conductances. *A*: *I-V* relationship of the *N*-methyl-D-aspartate (NMDA) conductance. *B*: superimposed model and experimental records of a biexponentially decaying γ-aminobutyric acid-A ($GABA_A$)-mediated inhibitory postsynaptic current (IPSC) measured at the cell body. Experimental response was evoked by stimulation in layer Ia. Model response was simulated by distributing 100 $GABA_{A,fast}$ ($\bar{g}_F$ = 1.15 nS) and 100 $GABA_{A,slow}$ ($\bar{g}_S$ = 0.25 nS) conductances over middle and distal apical dendritic segments of *cell 40C2*. *C*: superimposed experimental and simulated $GABA_B$-mediated inhibitory postsynaptic potentials (IPSPs) measured at the cell body. The $GABA_B$-mediated IPSP was isolated experimentally by addition of 6,7-dinitroquinoxaline-2,3-dione, 2-amino-5-phosphonovaleric acid (APV), and bicuculline to the bathing medium. Simulated response was obtained with 100 $GABA_B$ synapses ($\bar{g}_B$ = 0.03 nS) distributed randomly on apical dendrites at 100–600 μm from the cell body.

three types of GABAergic conductance that have been described in piriform cortex: the fast-decaying $GABA_A$ conductance ($GABA_{A,fast}$), the slow-decaying $GABA_A$ conductance ($GABA_{A,slow}$), and the $GABA_B$ conductance (Fig. 1) (Kapur et al. 1997; Tseng and Haberly 1988). Synaptic conductances were repetitively activated in bursts of four events at 50 or 100 Hz. This paradigm matches the stimulus bursts used to induce LTP and to study GABAergic modulation of the NMDA component in piriform cortex (Kanter et al. 1996). In addition, it simulates the input to rat piriform cortex elicited by natural odor stimulation that consists of brief 50-Hz oscillatory bursts during each sniff cycle (Adrian 1942; Ketchum and Haberly 1993a).

EXCITATORY CONDUCTANCES. The rising phase of the AMPA conductance (G_A) was approximated with a linear function of duration 0.5 ms; decay was exponential with a time constant of 2.0 ms (Ketchum and Haberly 1993b). The decay time constant of 1 ms used in the study of Ketchum and Haberly was increased to 2 ms to replicate the present responses, which were recorded at 29°C.

$$G_A = \bar{g}_A \cdot \text{rate} \cdot t, \quad t < 0.5 \text{ ms}$$

$$= \bar{g}_A \cdot \exp(-t/\tau), \quad t \geq 0.5 \text{ ms}$$

where $\bar{g}_A$ is the maximal AMPA conductance (nS), rate = 2 ms^{-1}, and τ = 2 ms. The reversal potential of the AMPA-mediated excitatory postsynaptic potential (EPSP) was 0 mV.

The NMDA conductance (G_N) was a sigmoidal function of membrane voltage (V_m) (Jahr and Stevens 1990a,b; Zador et al. 1990).

$$G_N = \bar{g}_N \frac{\exp(-t/\tau_1) - \exp(-t/\tau_2)}{1 + \eta \cdot [Mg^{2+}] \cdot \exp(-\gamma \cdot V_m)}$$

where $\bar{g}_N$ is the maximal NMDA conductance (nS), τ_1 = 60 ms, τ_2 = 0.66 ms, η = 0.33/mM, $[Mg^{2+}]$ = 1 mM, and γ = 0.08/mV. The 60-ms decay time constant of the NMDA conductance provided a good fit to the time course of the NMDA-mediated EPSP recorded intracellularly from pyramidal cells in layer II at 29°C (Kanter et al. 1996). The value of γ, which determines the dependence on voltage (from Mg^{2+} block), was a critical parameter in the simulations. With γ = 0.08/mV, the current through the channel at −60 mV [assumed reversal potential for the $GABA_A$ inhibitory postsynaptic potential (IPSP)] was ~20% of the maximum inward current, which occurred at approximately −20 mV (Fig. 1*A*). This is in the range reported in physiological studies (Hestrin et al. 1990; Perouansky and Yaari 1993; Stern et al. 1992). Reversal potential of the NMDA-mediated EPSP (E_{rev}) was 0 mV.

INHIBITORY CONDUCTANCES. $GABA_A$-mediated conductances (Fig. 1*B*) were modeled with exponential rising and falling phases. The $GABA_{A,fast}$ (G_F) and the $GABA_{A,slow}$ (G_S) conductances were

$$G_F = \bar{g}_F \cdot [1 - \exp(-t/\tau_{F1})] \cdot \exp(-t/\tau_{F2})$$

$$G_S = \bar{g}_S \cdot [1 - \exp(-t/\tau_{S1})] \cdot \exp(-t/\tau_{S2})$$

where $\bar{g}_F$ and $\bar{g}_S$ are the maximal conductances, τ_{F1} = 1.5 ms, τ_{F2} = 7.25 ms, τ_{S1} = 0.75 ms, and τ_{S2} = 37 ms. The reversal potentials of both $GABA_{A,fast}$ and $GABA_{A,slow}$ IPSP components were −60 mV (Kapur et al. 1997). IPSCs recorded from layer II pyramidal cells with whole-cell patch pipettes (Kapur et al. 1997) were used to determine the time constants for the model conductances.

The $GABA_B$ conductance (G_B; Fig. 1*C*) was modeled as an alpha function

$$G_B = \bar{g}_B \cdot \kappa \cdot t \cdot \exp(-t/t_p)$$

where $\bar{g}_B$ is the maximal conductance, $\kappa = e/t_p$, and t_p = 70 ms. Onset latency of the $GABA_B$ conductance was 50 ms, simulating the delayed onset of this process as recorded in layer II pyramidal cells in vitro. The reversal potential of the $GABA_B$ IPSP was −90 mV (Tseng and Haberly 1988).

RESULTS

Development of a compartmental model

Two superficial pyramidal cells with cell bodies in layer II (*40C2* and *37C1*) were reconstructed serially. The original drawing and compartmental representations for the cell that was used for the simulation of synaptic processes (*40C2*) are illustrated in Fig. 2.

Estimates of the cable parameters, R_m, C_m, and R_i, were derived by application of the constrained inverse computation (CIC) method of Holmes and Rall (1992) to reduced compartmental representations (Fig. 2C) of *cells 37C1* and *40C2* that consisted of a tapered cylinder with 20 compartments (see APPENDIX A). It was assumed that these parameters are uniform in all parts of pyramidal cells. Experimental values for R_N, τ_0, and C_0 used for these calculations were derived from voltage transients evoked by the onset and/or offset of small hyperpolarizing current pulses (Table 1). An example of a biexponential fit to an offset transient used to compute τ_0 and C_0 is illustrated in Fig. 3*A*.

For responses for which convergence was obtained, R_m varied from 14,005 to 16,134 Ωcm^2, C_m from 1.23 to 1.63 $\mu F/cm^2$, and R_i from 75 to 148 Ωcm (Table 1). The high sensitivity of computed values for R_i on R_N and C_0 was

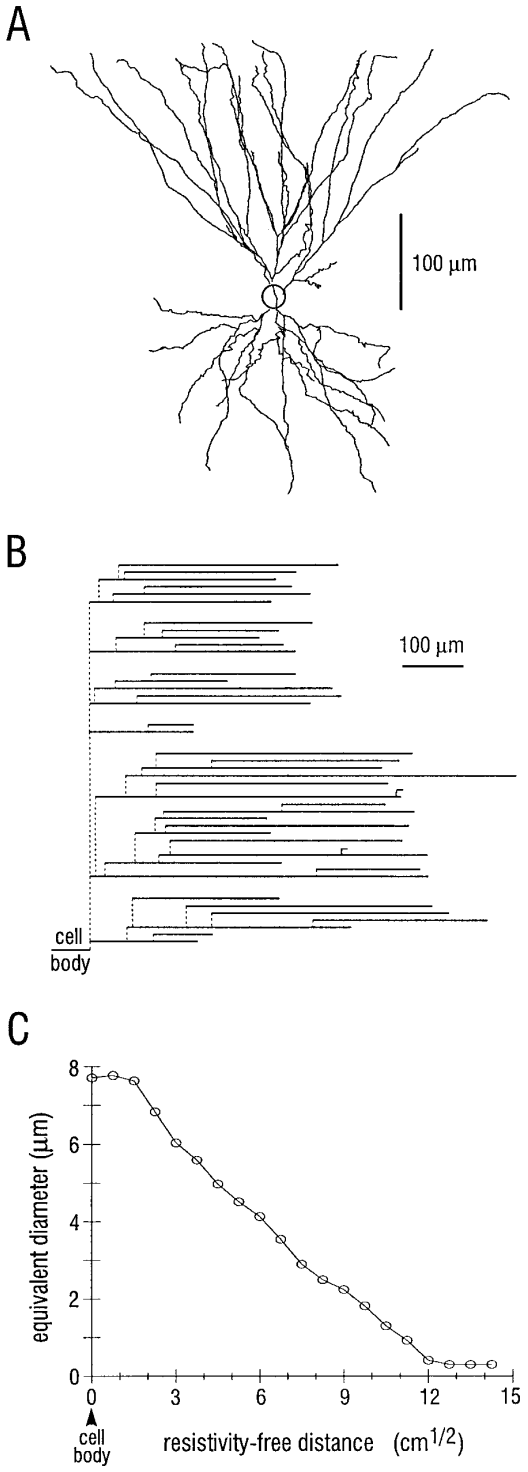

FIG. 2. Morphological reconstruction of a superficial pyramidal cell stained by diffusion of neurobiotin from a whole cell patch pipette (*cell 40C2*). *A*: dendritic tree projected in the coronal plane; position of the cell body is indicated by the circle; the apical dendritic tree extends upward. *B*: ''full morphology'' representation of *cell 40C2* with 344 cylindrical compartments in 43 dendritic branches. *C*: ''reduced morphology'' representation of *cell 40C2*. This consists of 20 dendritic compartments with a ''resistivity-free length'' (see text) of 75 μm and a cell body compartment identical to that in the full representation. Average diameter of each compartment of the tapering equivalent dendrite is plotted against ''resistivity-free distance'' from the cell body. Equivalent diameter at a given resistivity-free distance was obtained by summing the 3/2 power of diameter over all dendrites at that distance.

responsible for the approximate twofold spread in estimates of this parameter (see APPENDIX C). Values of cable parameters were insensitive to the initial estimates of R_m, C_m, and R_i (widely separated starting points in parameter space gave the same result), indicating that the final estimates do not correspond to local minima. If the membrane area contributed by spines were taken into account, R_m would be increased by ~40% (19,750 Ωcm^2 for *cell 40C2*) and C_m would be decreased by ~30% (1.06 μF/cm^2 for *40C2*; see APPENDIX B).

EVALUATION OF COMPARTMENTAL MODEL. To estimate the extent of error introduced by use of the reduced morphology model in the forward computation step, values for R_N, τ_0, and C_0 derived from voltage responses generated with the reduced morphology model were compared with those generated with the full model, using the same cable parameters. The values for R_N, τ_0, and C_0 derived with the two models differed by $\leq$2%, thereby justifying use of the reduced model (Fig. 3*C*).

The accuracy of the CIC method for calculating cable parameters was evaluated as follows: first, the voltage response to a somatic current pulse was generated with the full morphology model for *cell 37C1*, using assumed values for the cable parameters (R_m = 16,050 Ωcm^2, C_m = 1.52 μF/cm^2, and R_i = 100 Ωcm). This simulated voltage response then was analyzed as if it were an experimentally derived response. This entailed a determination of values for R_N, τ_0, and C_0 from the simulated voltage trace, and application of the CIC method using these values and the reduced morphology model to compute values for the cable parameters. Accuracy of the method then was assessed by comparing these computed values for cable parameters with the original assumed values. The estimates for R_m and C_m (16,134 Ωcm^2 and 1.51 μF/cm^2, respectively) were within 1% of the correct values, and R_i (118 Ωcm) was overestimated by 18%.

Values for cable parameters derived by the CIC method allowed accurate replication of physiological data as illustrated in Fig. 3*B*. The superimposed responses in this figure are an actual voltage transient from *cell 37C1* and a simulated transient from the full morphology representation obtained with cable parameters derived from the reduced representation.

Simulation of synaptic processes

GABAERGIC REGULATION OF THE NMDA COMPONENT. The simulations of synaptically mediated responses were carried out on the fully branched model for *cell 40C2* (Fig. 2). Visual comparison of the morphology of this cell with a large sample of other intracellularly stained cells suggests that it is representative of the majority of superficial pyramidal cells. The cell was divided into 345 cylindrical compartments (Fig. 2*B*), each representing a dendritic segment $\leq$35 μm in length.

Study of the effects of dendritic IPSCs on NMDA-mediated current and voltage was carried out on a distal apical dendritic compartment of the full morphology model that contained NMDA (Fig. 1*A*), AMPA, and GABA (Fig. 1, *B* and *C*) conductances. Leakage conductance (R_m) was distributed uniformly in all compartments. For this analysis, it was assumed

TABLE 1. *Estimates of cable parameters for cells 40C2 and 37C1 obtained with the constrained inverse computation method*

Cell	Pulse Amp, nA	Pulse Onset/Offset	R_N, MΩ	τ_0, ms	C_0, mV	R_m, Ωcm^2	C_m, μF/cm^2	R_i, Ωcm
37C1	−.01	onset	92.62	19.32	0.88	*	*	*
	−.01	offset	92.62	17.59	−.83	14,321	1.23	148
	−.015	onset	89.71	22.62	1.24	14,265	1.59	107
	−.015	offset	89.71	23.66	−1.26	14,497	1.63	86
	−.02	onset	101.06	24.32	1.86	16,048	1.52	122
	−.02	offset	101.06	25.17	−1.92	16,570	1.52	75
40C2	−.02	offset	74.5	20.82	−1.32	14,005	1.49	137

* Responses did not converge.

that when excitatory and inhibitory conductances are distributed uniformly at relatively high densities, results from the analysis of synaptic interactions in a single compartment are applicable to the entire dendritic tree. By placing both excitatory and inhibitory conductances in the same compartment, the maximum extent of interaction could be assessed.

To assess the influence of time course of IPSCs on their effectiveness for controlling the NMDA component, the magnitudes of inhibitory conductances were set relatively high ($\bar{g}_F$ = 5 *nS*, $\bar{g}_S$ = 5 *nS*, $\bar{g}_B$ = 0.2 nS) so that all three types of IPSCs could control the membrane potential. NMDA and AMPA conductances were varied to study the effects of inhibition on strong and weak excitatory inputs. All synapses were activated with a burst of four inputs at 50 or 100 Hz. Current through the NMDA channel and voltage in the dendritic compartment that contained the synaptic conductances were monitored. Charge transfer through the NMDA channel when all GABAergic IPSCs were present (''fully inhibited case''), was normalized to 1. Starting values for cable parameters were: R_m = 14,005 Ωcm^2, C_m = 1.49 μF/cm^2, and R_i = 137 Ωcm.

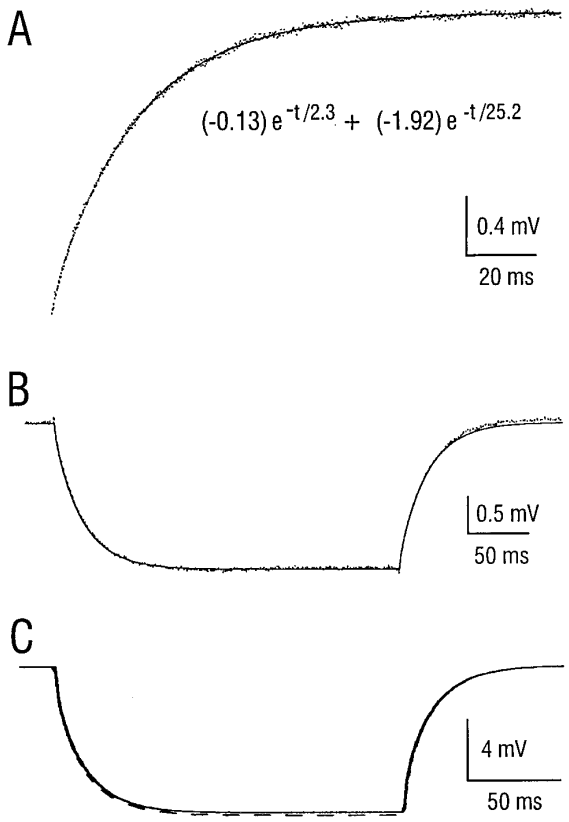

FIG. 3. Sample experimental and simulated voltage transients for superficial pyramidal cell models. *A*: method for extraction of membrane time constant, τ_o (longest time constant), and its coefficient, C_0, from experimental voltage transients evoked by hyperpolarizing current pulses. A biexponential fit (——) is superimposed on the decay phase of the voltage response (●) to a −0.02 nA somatic current pulse (*cell 37C1*). *B*: comparison of voltage responses generated in the full morphology model with responses measured experimentally (*cell 37C1*). Actual and simulated responses at the soma to a somatic current pulse (−0.02 nA) are superimposed. *C*: comparison of somatic voltage responses generated in the full morphology and reduced morphology models of *cell 40C2*. Values of R_N, τ_0, and C_0 computed from these simulated voltage transients differed by <2%.

The results with a strong NMDA conductance (g_N = 2.4 nS and g_A = 1.2 nS) are illustrated in Fig. 4*A*. In this case, blockade of GABAergic inhibition resulted in a large increase in NMDA current over the fully inhibited case. In the absence of all inhibition, there was summation to a large ''envelope'' of current through the NMDA channel (Fig. 4*A1*). Comparison of the efficacies of the different types of GABAergic IPSCs revealed that the $GABA_{A,fast}$ IPSC alone could block membrane depolarization during the early portion of the burst-evoked EPSP (Fig. 4*A2*). However, because $GABA_{A,fast}$ terminated before the NMDA-mediated EPSC, the NMDA current increased during the latter portion of the burst. The $GABA_B$ IPSC alone had little effect on membrane potential or the NMDA current because of its late onset (50-ms latency; peak at 150 ms). However, $GABA_{A,slow}$ alone could restrain changes in membrane potential throughout the burst and, therefore, was the most effective at regulating current flux through the NMDA channel.

Charge transfer increased 3.9-fold when all GABAergic IPSCs were blocked (Fig. 5, ▨). The $GABA_B$ IPSC reduced this charge transfer by ~25%, the $GABA_{A,fast}$ IPSC by ~35%, whereas the $GABA_{A,slow}$ IPSC alone reduced it by >70%. A combination of $GABA_{A,fast}$ and $GABA_B$ IPSCs also reduced charge transfer ~70%.

When the same intermediate value for maximum conductance (1.2 nS) was assigned to both NMDA and AMPA channels, blockade of all IPSCs again caused an approximate fourfold increase in charge transfer through the NMDA channel (not illustrated), and the $GABA_B$ IPSC by itself reduced this charge transfer by a small amount (~30%). However, $GABA_{A,fast}$ alone was now as effective as $GABA_{A,slow}$ in reducing charge transfer (67% by $GABA_{A,fast}$ and 69% by $GABA_{A,slow}$. The weaker NMDA conductance in this case was unable to depolarize the membrane after the $GABA_{A,fast}$ IPSC had terminated.

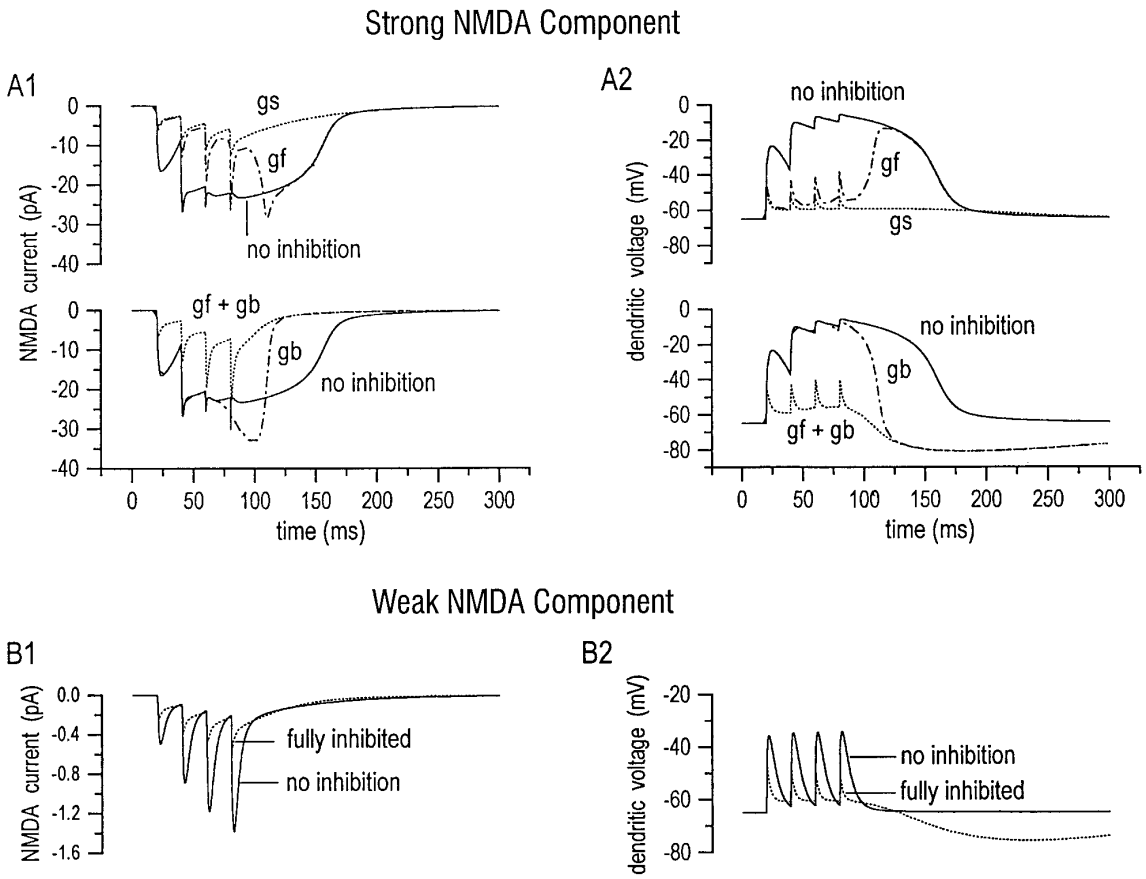

FIG. 4. GABAergic regulation of NMDA current and resulting dendritic potential. Synaptic conductances were placed in a single distal apical dendritic compartment of *cell 40C2* at a distance of 485 μm from the cell body; leakage conductance (R_m) was distributed uniformly in all compartments of the model cell. Activation was with a four-pulse, 50-Hz burst. *Left*: current through the NMDA channel. *Right*: membrane potential of the dendritic compartment with the synaptic conductances. *A*: regulation of a strong NMDA conductance ($\bar{g}_N$ = 2.4 nS) by various combinations of inhibitory conductances. *A1*: comparison of NMDA current in the absence of inhibition with NMDA current in the presence of $GABA_{A,slow}$ alone (gs), $GABA_{A,fast}$ alone (gf), $GABA_B$ alone (gb), and $GABA_{A,fast}$ plus $GABA_B$ (gf + gb). *A2*: same as *A1* but for dendritic potential. Note the summation of the NMDA current and membrane potential during burst stimulation in the absence of inhibition and the effective blockade of this potential by $GABA_{A,slow}$ alone. *B*: regulation of a weak NMDA conductance ($\bar{g}_N$ = 0.1 nS) by various inhibitory conductances. *B1*: current through the NMDA channel with full inhibition (gs, gf, and gb) and with no inhibition. *B2*: same as *B1* but for dendritic potential. Note the lack of summation of NMDA current or resulting potential in the absence of inhibition that precluded a substantial effect from blockade of inhibition. Time scale in *A* also applies to *B*.

When the NMDA conductance was weak relative to the AMPA conductance ($\bar{g}_N$ = 0.1 nS vs. $\bar{g}_A$ = 1.2 nS), blockade of all inhibitory conductances potentiated current flux through the NMDA channel by only 1.6-fold over the fully inhibited case (Fig. 4*B1;* ■ in Fig. 5). Block of inhibition resulted in only a transient increase in NMDA current that matched the time course of the AMPA-mediated EPSC (Fig. 4*B1*). The NMDA conductance in this case was not strong enough to contribute sufficient depolarization by itself to remove the Mg^{2+} block, even in the absence of inhibition (Fig. 4*B2*, note lack of summation during the burst). When the AMPA conductance was doubled to 2.4 nS, transfer through the NMDA channel for either a 50- or a 100-Hz burst was increased only by an additional 25% (not illustrated).

GABAERGIC REGULATION OF ASSOCIATIVE INTERACTIONS. In piriform cortex, block of $GABA_A$-mediated inhibition is required for the induction of associative LTP by simultaneous activation of afferent and association fibers that terminate on adjacent apical dendritic segments (Kanter and Haberly 1993) or independent sets of association fibers that terminate in close proximity (Jung and Larson 1994). The paradigm used for these studies was that developed in the hippocampus where a weak stimulus to one set of excitatory fibers is paired with a strong stimulus to an independent set (Barrionuevo and Brown 1983; Levy and Steward 1979). The weak stimulus alone results in no change in synaptic efficacy, but when paired with the strong stimulus in the presence of a $GABA_A$ antagonist, NMDA-dependent LTP of the weak input is induced.

To study the mechanism of this effect, weak excitatory, strong excitatory, and GABAergic inputs were placed on the same dendritic compartment as in the above simulations. The placement of strong and weak excitatory inputs on the same compartment insured that the depolarization generated by the strong input reached the site of the weak. Effects of spatially separating the weak and strong inputs were not explored. The strong excitatory input consisted of 1 nS maximum conductances for both the AMPA and NMDA channels. The weak input consisted of a 0.3-nS maximum con-

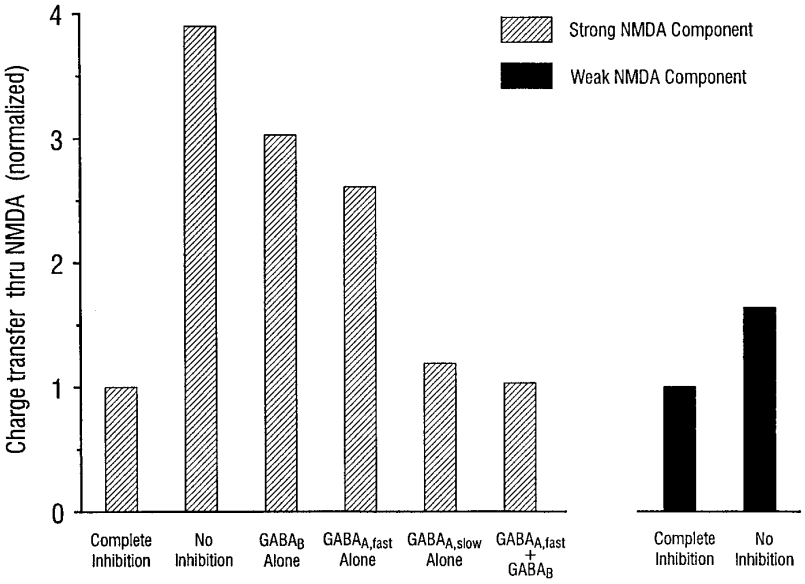

FIG. 5. Inhibition of charge transfer through simulated NMDA channels by $GABA_{A,fast}$-, $GABA_{A,slow}$-, and $GABA_B$-mediated IPSCs. Values for charge transfer are normalized to the complete inhibition conditions for weak and strong NMDA activation.

ductance for the AMPA channel and 0.1 nS for the NMDA channel. Maximum conductances of the GABAergic synapses were the same used in the above simulations ($\bar{g}_F$ = 5 nS, $\bar{g}_S$ = 5 nS, and $\bar{g}_B$ = 0.2 nS). Synapses were activated in 50-Hz bursts of four pulses. Results of this study are illustrated in Figs. 6 and 7. Figure 6*A* shows the current through the NMDA component of the weak excitatory input, and Fig. 6*B* shows potential in the compartment that contained the model synapses.

Charge transfer through the NMDA conductance when the weak excitatory input was activated alone (no IPSPs or strong excitatory input) was almost identical to the charge transfer through this channel in the fully inhibited case with the strong excitatory input present (solid bar and first hatched bar in Fig. 7). As described above, this result stems from the inability of the weak input to depolarize the membrane sufficiently to remove the Mg^{2+} block (Fig. 6*B*). By contrast, in the absence of inhibition, simultaneous activation of weak and strong excitatory inputs produced a 3.7-fold increase in charge transfer through the weak NMDA channel in comparison with the fully inhibited case (hatched bars in Fig. 7). Because the conductance of the strong NMDA synapse was in the intermediate range as defined in the previous analysis ($\bar{g}_N$ = 1 nS), both $GABA_{A,fast}$ and $GABA_{A,slow}$ IPSCs were almost equally effective in reducing the membrane depolarization and consequently the charge transfer through the weak NMDA channel. The presence of either IPSC reduced charge transfer by ~65% relative to the inhibition-free case. The $GABA_B$ IPSC was much less effective in controlling the depolarization evoked by the burst (charge transfer was reduced by ~30% in the presence of this IPSC).

SELECTIVE MODULATION OF EXCITABILITY BY SOMATIC-REGION INHIBITION. By locally applying bicuculline in a slice preparation, it has been shown that the dendritic $GABA_A$-mediated IPSP is sufficient to block the NMDA-mediated depolarization evoked by burst stimulation of afferent fibers (Kanter et al. 1996). This demonstration suggests the hypothesis that regulation of NMDA-dependent LTP is accomplished by selective control of dendritic inhibition. For this

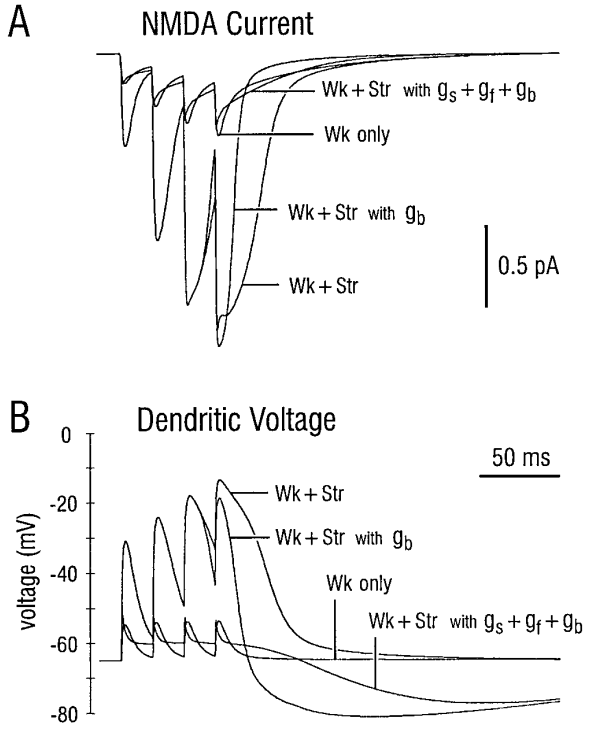

FIG. 6. GABAergic modulation of the potentiation of the NMDA component of a weak excitatory input by a concomitant strong excitatory input. Simulations were carried out in a distal dendritic compartment of *cell 40C2* with weak (Wk) and strong (Str) excitatory inputs and $GABA_{A,slow}$ (gs), $GABA_{A,fast}$ (gf), and $GABA_B$ gb) inhibitory conductances. For the weak excitatory input, $\bar{g}_A$ = 0.3 nS and $\bar{g}_N$ = 0.1 nS; for the strong excitatory input, $\bar{g}_A$ = 1.0 nS and $\bar{g}_N$ = 1.0 nS. *A*: current through the NMDA component of the weak excitatory input presented alone (Wk only), when paired with the strong input in the absence of inhibition (Wk + Str), when paired with the strong input in the presence of all inhibitory components (Wk + Str with gs + gf + gb), and when paired with the strong input in the presence of the $GABA_B$ component alone (Wk + Str with gb). *B*: same as *A* but for dendritic membrane potential.

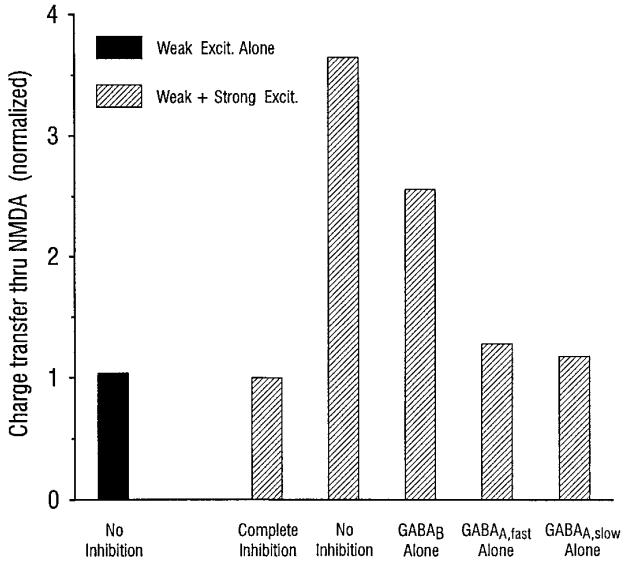

FIG. 7. Inhibitory modulation of the extent of increase in charge transfer through the NMDA component of a weak excitatory input when paired with a strong input. Values for charge transfer are normalized to the complete inhibition condition for paired weak and strong excitation.

mechanism to be feasible, two conditions would have to be met: first, the increased excitability resulting from block of dendritic inhibition would have to be balanced by a selective increase in the somatic-region IPSC to prevent epileptiform bursting to which piriform cortex is highly susceptible. This would be taken care of automatically by the feedback configuration of the circuitry that mediates the somatic-region IPSC. Second, the somatic-region IPSC would have to be able to effectively control firing while having little effect on the NMDA component in dendrites. This latter condition, which would be difficult to test experimentally,[1] was investigated with the model pyramidal cell. The hypothesis tested was that a somatic IPSC can be of sufficient strength to block the generation of action potentials without compromising a NMDA component that has been enabled by block of dendritic inhibition.

To test this hypothesis, 100 AMPA ($\bar{g}_A$ = 0.5 nS) and 100 NMDA ($\bar{g}_N$ = 0.3 nS) excitatory synaptic components were distributed widely on the distal half of the dendritic tree of the model cell ($\geq$275 μm from the soma) to represent the afferent fiber input (● in Fig. 8*C, 1* and *2*). The AMPA and NMDA conductances were colocalized on dendritic compartments that were chosen at random within the distal dendritic region.

The distribution of GABA$_{A,fast}$ and GABA$_{A,slow}$ components was adjusted for best-fit to a representative biexponentially decaying IPSC evoked by shock stimulation in layer Ia (Fig. 1*B*). The optimal distribution consisted of 100 GABA$_{A,fast}$ conductances on apical dendritic compartments at a distance of 100–400 μm from the cell body, and 100 GABA$_{A,slow}$ conductances at a distance of 200–600 μm (○ in Fig. 8*C2*). Maximum conductance for GABA$_{A,fast}$ was 1.15 nS; for GABA$_{A,slow}$ the maximum was 0.25 nS.

[1] Activation of a somatic IPSC of sufficient strength to block spike generation would not allow the visualization of dendritically generated EPSPs from somatic recording sites.

GABA$_B$ input was simulated with 100 model synapses with a maximum conductance of 0.03 nS that were distributed randomly on apical dendritic compartments at 100–600 μm from the soma. This distribution was chosen on the basis of physiological evidence indicating that this IPSC is small or absent in the vicinity of the cell body (Tseng and Haberly 1988).

An inactivating Na^+ conductance and a delayed rectifier K^+ conductance were added to the soma compartment to simulate Na^+ spikes. Threshold was −54 mV, the approximate level observed under the present recording conditions (A. Kapur, unpublished data). Membrane potential at the soma, the average membrane potential in the distal half of the apical dendritic tree, and the total current through all the NMDA channels were monitored.

In the absence of any GABA$_A$-mediated inhibition, activation of excitatory synapses on distal dendrites with a burst of four inputs at 50 Hz evoked repetitive spiking at the soma (Fig. 8*A1*) and a large depolarization in the distal dendrites (Fig. 8*B1*). With GABAergic inhibition at the soma alone (GABA$_{A,slow}$, $\bar{g}_S$ = 30 nS) and the same pattern of dendritic excitatory input, spiking at the soma could be blocked (Fig. 8*A2*) with little effect on dendritic depolarization (Fig. 8*B2*). GABA$_{A,slow}$ was used for these tests at the soma because, as shown above, it was most effective in regulating strong NMDA currents. Dendritic GABAergic inhibition could block the NMDA-mediated depolarization in the dendrites (note the lack of summation in Fig. 8*B3*) and, consequently, spiking at the soma (Fig. 8*A3*). In the absence of all GABA-mediated inhibition, total charge transfer through NMDA channels was 2.26 times that with dendritic GABA$_A$-mediated inhibition. When somatic GABA$_A$-mediated inhibition was activated, this factor decreased only slightly (to 2.06 times that with dendritic inhibition). The decrease would be even less for somatic IPSCs consisting primarily of a fast component as observed experimentally (Kapur et al. 1997). Similar results were obtained when the neuron was made more electrotonically compact by lowering R_i from 137 to 75 Ωcm—the lower limit of computed values for this parameter. It is concluded that somatic GABAergic inhibition can effectively regulate the generation of action potentials while having little effect on the NMDA component of EPSPs.

DISCUSSION

A compartmental model was developed for superficial pyramidal cells in piriform cortex to study aspects of the interaction of IPSCs with the NMDA component of EPSPs that are not readily accessible to physiological analysis. The results have provided support for a specific role of GABAergic inhibition in regulation of the NMDA component and suggest that the independence and differing properties of dendritic and somatic inhibition provide a mechanism whereby such regulation of the NMDA component or other dendritic processes could be accomplished without increasing the propensity for epileptiform bursting.

Compartmental model

USE OF A UNIFORM MEMBRANE RESISTIVITY MODEL. Experimental responses to voltage transients could be reproduced

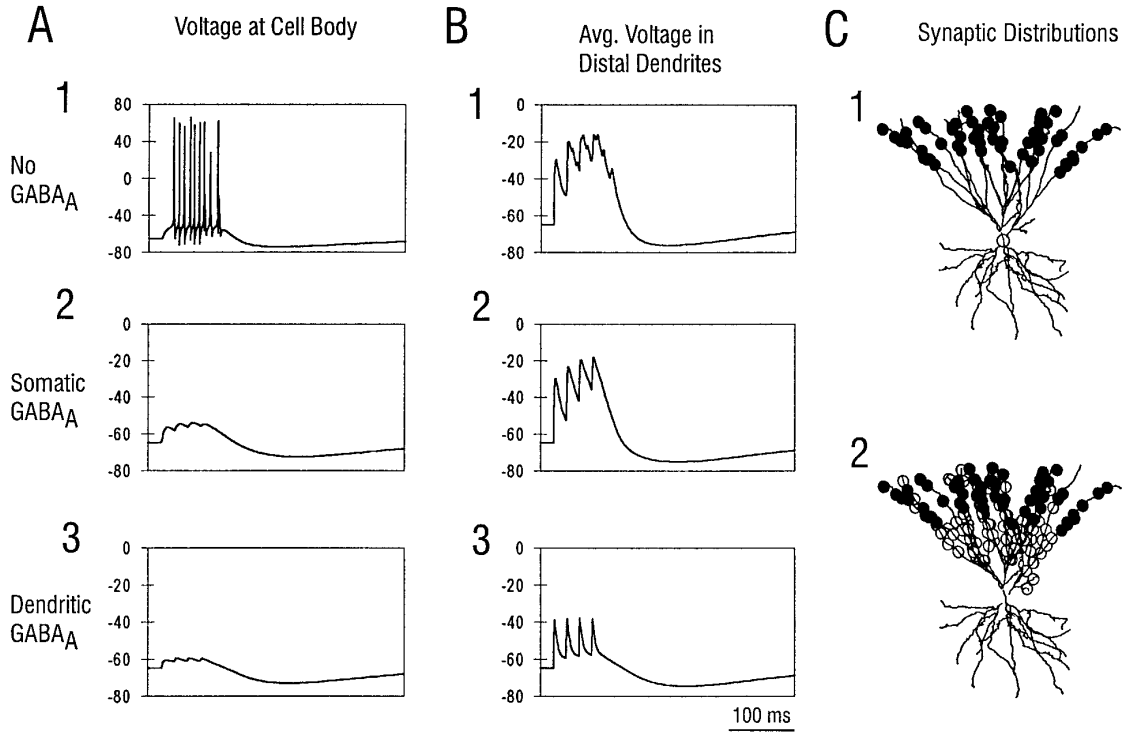

FIG. 8. Dendritic but not somatic $GABA_A$ inhibition blocks the NMDA component of excitatory postsynaptic potentials. For all illustrated simulations, 100 α-amino-3-hydroxy-5-methyl-4-isoxazolepropionic acid (AMPA) and 100 NMDA conductances (● in *C1* and *C2*) were colocalized on the distal half of the apical dendritic tree of *cell 40C2*, 100 $GABA_B$ conductances were distributed over the apical dendritic tree starting at 100 μm from the cell body (not shown), and an inactivating Na^+ conductance and delayed rectifier were inserted into the soma to generate action potentials. Somatic $GABA_A$ inhibition consisted of $GABA_{A,slow}$ alone to maximize its effect on the NMDA component; dendritic $GABA_A$ inhibition consisted of a distribution of $GABA_{A,fast}$ and $GABA_{A,slow}$ conductances (○ in *C2*) that generated a biexponentially decaying IPSC that matched a representative physiological recording (see text for details). Stimulation was with a 50-Hz, four-pulse burst. *A* is voltage in the somatic compartment; *B* is average voltage in the distal half of the apical dendrite. *A*: when no $GABA_A$ conductance was present, burst activation of the excitatory and $GABA_B$ conductances evoked spiking at the soma (*A1*) and a large depolarizing ''envelope'' in the apical dendrite (*B1*). When $GABA_A$ conductance was present at the cell body alone, spiking was blocked (*A2*) with minimal effect on the large depolarization envelope in dendrites (*B2*). When $GABA_A$ conductance was present on the apical dendrite but not the cell body, the NMDA-mediated depolarizing envelope in the dendrites was blocked (*B3*) in addition to a block of spiking (*A3*).

with a compartmental model that did not contain a somatic shunt (a lower value of R_m for the somatic compartment). Recent studies on CA3 pyramidal neurons (Jonas et al. 1993; Major et al. 1994) and on interneurons in the CA1 region (Thurbon et al. 1994) also have found that a somatic shunt may be unnecessary to fit data obtained with the whole cell recording technique. However, it has been demonstrated for whole cell data (Major et al. 1994), as well as certain data obtained with sharp microelectrodes (Nitzan et al. 1990), that adequate fits to voltage transients can be obtained both with and without somatic shunts. The effect of including a shunt would be to increase estimates of dendritic R_m and slightly reduce estimates of C_m and R_i.

COMPARISON WITH HIPPOCAMPAL PYRAMIDAL NEURONS. Comparison of values from the present study to those for hippocampus reveals a close similarity in membrane properties between pyramidal cells in piriform cortex and those in CA1 but marked differences in some parameters for CA3 pyramids (Major et al. 1994; Turner 1984). In the two cells from piriform cortex examined in this study and in a third cell that was reconstructed serially, the total membrane area ranged from 24,294 to 33,311 μm^2 (assuming spines contributed 29% of the total membrane area). By comparison, the total neuronal membrane area of CA1 cells was estimated as 24,400 μm^2 (Turner 1984), whereas that of CA3 cells was estimated as 47,000 μm^2 (Turner 1984) and 59,900 μm^2 (Major et al. 1994). The membrane time constant was ~20 ms in piriform pyramidal cells (with $V_m = -73$ to -75 mV), 23 ± 2 ms (mean ± SE) in CA1 pyramids (with $V_m = -70$ mV) and 61 ± 4 ms in CA3 pyramids ($V_m = -69$ mV) (Spruston and Johnston 1992). The input resistance for all three cell types was similar (order of 75–125 MΩ).

Estimates of R_m in piriform pyramidal cells (14.0–16.6 $k\Omega cm^2$, Table 1; 19.7 $k\Omega cm^2$ for *cell 40C2* after correction for spine area, APPENDIX B) were again similar to reported values for CA1 pyramids (17.9–28 $k\Omega cm^2$ with assumed $C_m = 1\ \mu F/cm^2$) (Spruston and Johnston 1992; Turner 1984), and lower than those for CA3 pyramidal cells (66–200 $k\Omega cm^2$, with $C_m = 1\ \mu F/cm^2$) (Major et al. 1994; Spruston and Johnston 1992).

A recent study on CA3 pyramidal cells concluded that C_m is ~0.7 $\mu F/cm^2$—substantially lower than the usual assumed value of 1 $\mu F/cm^2$ (Major et al. 1994). Similar values were reported in earlier studies of other types of neurons

and nonneuronal cells (Fettiplace et al. 1971; Haydon et al. 1980; Takashima 1976). In the present study, the value for C_m computed for *cell 40C2* after correction for spine membrane area (1.06 $\mu F/cm^2$, APPENDIX B), was close to the traditional value. However, in view of the uncertainties in the light microscopic measurements of spine dimensions on which this estimate depends, a value on the order of 0.7 $\mu F/cm^2$ cannot be ruled out.

GABAergic regulation of the NMDA component

MECHANISM. When an IPSC occurs concomitantly with an EPSC, the resulting EPSP is reduced in amplitude as a consequence of current ''shunting''. The shunting process is an indirect one[2] whereby the depolarizing shift in membrane potential resulting from the EPSC alters the driving force on the inhibitory channels, eliciting an outward current, even when the reversal potential for the IPSC is depolarized with respect to resting potential as in piriform cortex (Scholfield 1978). The potential change generated by the outward current sums with that evoked by the inward excitatory current, resulting in a decrease in EPSP amplitude. Because EPSP amplitude cannot be decreased below the reversal potential for the $GABA_A$-mediated IPSC, the position of this reversal relative to the *I-V* relationship for the NMDA channel (Fig. 1*A*) is an important variable. Unfortunately, the true value for the $GABA_A$ reversal is uncertain because of the effects of bathing medium composition, pipette electrolyte, the age of animals, and a possible difference in dendrites and cell bodies. For the present study, a conservative value of -60 mV was assumed based on findings in piriform cortex slices from mature animals obtained with sharp micropipettes (Tseng and Haberly 1988). However, findings obtained in vivo suggest that this value may be as high as -70 mV in intact animals (Haberly, unpublished data); this could substantially increase the capacity of $GABA_A$-mediated inhibition to regulate the NMDA component.

Inhibition regulates current through NMDA channels by regulating the resulting level of depolarization. Comparison of responses to the first and later stimuli in bursts like those used to induce LTP, reveals that the effects of GABAergic inhibition on both NMDA current and membrane potential are accentuated greatly by repetitive activation (Fig. 4*A*, *1* and *2*).

RELATIVE EFFECTIVENESS OF $GABA_{A,FAST}$, $GABA_{A,SLOW}$, AND $GABA_B$ CONDUCTANCES. The results showed that for strong EPSCs, only $GABA_{A,slow}$ could block effectively the NMDA component. Weaker NMDA components also could be blocked by $GABA_{A,fast}$ because the tail of the NMDA conductance was not strong enough to depolarize the membrane even in the absence of inhibition. As a result of its long latency and slow time course, the $GABA_B$-mediated IPSC had a modest effect on NMDA current regardless of the strength of EPSCs.

Experimental studies also have shown that the presence of postsynaptic $GABA_B$-mediated inhibition alone cannot prevent the induction of associative LTP, whereas $GABA_A$-mediated inhibition alone can (Kanter and Haberly 1993). In addition, the NMDA response to burst stimulation is enhanced greatly after $GABA_A$ blockade but not after $GABA_B$ blockade (Kanter et al. 1996). However, interpretation of these experimental results is complicated by the presence of presynaptic $GABA_B$ receptors the block of which by antagonists could increase GABA release thus offsetting the effect of block of postsynaptic $GABA_B$ receptors.

ROLE OF THE AMPA COMPONENT IN NMDA REGULATION. An important question is the extent to which current through NMDA channels can be enabled by the depolarization evoked by a coactivated AMPA component. In the simulations, the activating effect of the AMPA component on charge transfer was modest (1.6-fold) because of its brief duration. Inclusion of frequency potentiation of the AMPA component in the simulations would have had little effect, as indicated by the 25% increase in NMDA current that resulted from a doubling of AMPA conductance.

EXTENT OF INCREASE IN NMDA CURRENT AND FREE CALCIUM. The simulations indicated that charge transfer through NMDA channels can be increased by up to fourfold during block of dendritic $GABA_A$ inhibition. Based on results of modeling studies (Gamble and Koch 1987; Holmes and Levy 1990; Zador et al. 1990), it appears that the resulting increase in free Ca^{2+} that is believed to trigger LTP would be much greater than fourfold. For example, simulations by Holmes and Levy (1990) concluded that a twofold increase in Ca^{2+} influx is amplified to a sevenfold increase in free Ca^{2+} in the spine head at 50 Hz and a threefold increase boosted to 30-fold at 200 Hz due to a transient saturation of fast Ca^{2+} buffering systems in spines. This compares with the two- to fourfold increase in free Ca^{2+} that has been estimated to be sufficient to trigger LTP (Neveu and Zucker 1996).

EFFECT OF GABAERGIC INHIBITION ON ASSOCIATIVE FACILITATION OF THE NMDA COMPONENT. Most studies with the associative LTP paradigm have found that the potentiation of weak inputs by concomitant strong bursts requires block of $GABA_A$-mediated inhibition (Gustafsson and Wigstrom 1986; Jung and Larson 1994; Kanter and Haberly 1993; Tomasulo et al. 1993; Zhang and Levy 1993). The present results support the hypothesis, based on experimental study in piriform cortex (Kanter et al. 1996), that facilitation of the NMDA component by block of the dendritic $GABA_A$ inhibition can enable potentiation of weak inputs when they occur concurrently with other inputs (also see Tomasulo et al. 1993; Zhang and Levy 1993). The need for disinhibition would be increased for spatially separated inputs.

In view of the highly distributed (divergent) nature of excitatory connections within the piriform cortex and the segregation of afferent and intrinsic excitatory connections on different apical and basal dendritic segments (Haberly 1997), it seems plausible that the learning of olfactory discriminations requires potentiation of multiple weak, spatially separated inputs as simulated by the associative LTP paradigm.

Control of neuronal function through selective regulation of spatially localized IPSCs

The results support the feasibility for control of neuronal processes through selective changes in excitability of inter-

[2] A common misconception is that a direct shunting of excitatory current takes place through open $GABA_A$ channels. This cannot occur as a result of the anion selectivity of the $GABA_A$ channel.

neurons that terminate at different sites on pyramidal cells. Increases or decreases in dendritic or somatic inhibition could be mediated through monoaminergic, cholinergic, or GABAergic fiber systems from the basal forebrain or brain stem that can modulate GABAergic inhibition via a variety of mechanisms and have been implicated in the control of learning and memory and many other functions (Aigner 1995; Dalmaz et al. 1993; Freund and Buzaki 1996; Hasselmo 1995; Nabeshina 1993; Sara et al. 1994; Steckler and Sahgal 1995). These systems terminate in piriform cortex, as in the hippocampus and neocortex (Haberly 1997). A specificity of action on dendritic or somatic inhibition could be achieved through selective expression of receptors or through a laminar selectivity in the termination of modulatory fiber systems. The indications that GABAergic inputs to distal dendritic and somatic regions of pyramidal cells in piriform cortex are derived at least partially from different populations of interneurons (Kanter et al. 1996; Kapur et al. 1997) indicate that selective action of neuromodulators could be achieved through changes in interneuron excitability rather than being limited to actions at the pyramidal cell level.

In addition to regulating synaptic plasticity by the postulated direct action on the NMDA component, dendritic $GABA_A$ tone also could play a role in synaptic plasticity by modulating the back propagation of action potentials into dendrites (Magee and Johnston 1997; Markram et al. 1997; Svoboda et al. 1997). Regulation of the NMDA component by dendritic inhibition would also influence the integration of synaptic inputs, particularly repetitive ones that can strongly activate this component. Dendritic inhibition also would be expected to modulate the activation of voltage-dependent Na^+ and Ca^{2+} channels (Gillessen and Alzheimer 1997; Lipowsky et al. 1996; Magee and Johnston 1995; Miles et al. 1996; Schwindt and Crill 1995) that may play a role in both integrative and plastic processes.

Inhibition in the somatic region (cell body or axon initial segment) is of obvious significance for preventing the development of seizure activity by virtue of its fast and strong feedback action on the initiation of action potentials, but it also may play a role in shaping cell output (see Fig. 6 in Pearce 1993). The present demonstration that somatic $GABA_A$ inhibition of sufficient strength to block the generation of action potentials can have little effect on NMDA expression in distal dendrites suggests that the more subtle changes that normally would be required to regulate system excitability would have minimal effect on integrative and plastic processes. However, if back-propagating action potentials in dendrites (Magee and Johnston 1997; Markram et al. 1997) prove to be an important factor in the induction of learning-related changes in synaptic efficacy, then somatic-region inhibition would play a role in its regulation. It could be speculated that effects of dendritic inhibition on synaptic plasticity dominate in distal dendrites that may not be invaded by Na^+ spikes, and the effects of somatic-region inhibition dominate in proximal dendrites. Clearly, the actions and differential regulation of spatially restricted inhibitory processes are of great complexity, but an understanding of these processes should provide important insights into normal functions and seizure disorders.

APPENDIX A

Procedures for development of the compartmental model

CONSTRUCTION OF A REDUCED MORPHOLOGY MODEL. To facilitate the estimation of cable parameters, a reduced morphology model consisting of a soma and tapered equivalent dendrite encompassing both apical and basal trees was constructed as described by Holmes and Rall (1992). This method was applied after preliminary tests revealed that an equivalent cylinder approximation cannot be made for these cells. To obtain the equivalent dendrite, a ''resistivity-free length'' (rfl) first was computed for each of the compartments used to represent the full branched morphology. The rfl of compartment n is given by $2l_n/d_n^{1/2}$, where l_n and d_n are the physical length and diameter of compartment n. Multiplication of rfl by $(R_i/R_m)^{1/2}$ yields electrotonic length. Next, a ''resistivity-free distance'' (rfd) of each compartment from the soma was computed, the rfd of the soma being set to 0. The rfd of compartment n is given by $rfd_n = rfd_p + rfl_n$ where $rfd_p = rfd$ of the parent compartment. The entire dendritic tree then was collapsed into a single unbranched dendrite, the diameter, d_{eq}, of which, as a function of the resistivity-free distance y, is given by $d_{eq}^{3/2}(y) = \Sigma\, d_j^{3/2}(y)$, where $d_j(y)$ is the diameter of dendrite j at resistivity-free distance y from the soma. The equivalent dendrite was tapered rather than cylindrical (Fig. 1) because Rall's 3/2 power law was not followed at many branch points and because dendrites terminated at different electrotonic distances from the soma.

APPLICATION OF THE CONSTRAINED INVERSE COMPUTATION METHOD. The two-step, iterative procedure of Holmes and Rall (1992) was used to estimate the cable parameters: membrane resistivity (R_m), membrane capacitance (C_m), and cytoplasmic resistivity (R_i). This process can be schematically depicted as follows

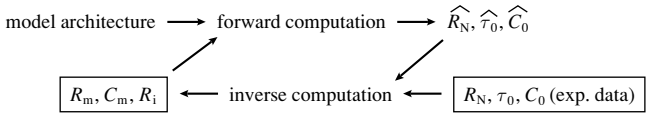

During the forward computation, values for input resistance, membrane time constant, and coefficient of the membrane time constant were computed by solving the compartmental model equations for a somatic current pulse input to the reduced morphology representation of pyramidal cells, using ''best-guess'' values for R_m, C_m, and R_i (for details, see Holmes and Rall 1992; Perkel et al. 1981). During the second step, termed the constrained inverse computation, the Newton-Raphson (N-R) algorithm (Press et al. 1992) was applied to refine the values for R_m, C_m, and R_i. The following functions were simultaneously zeroed with this multidimensional root finding algorithm

$$f_1 = (1/\tau_0)[\tau_0 - \widehat{\tau_0}(R_m, C_m, R_i)]$$
$$f_2 = (1/C_0)[C_0 - \widehat{C_0}(R_m, C_m, R_i)]$$
$$f_3 = (1/R_N)[R_N - \widehat{R_N}(R_m, C_m, R_i)]$$

where $\widehat{\tau_0}$, $\widehat{C_0}$ and $\widehat{R_N}$ are values of the membrane time constant, coefficient of the membrane time constant, and input resistance computed with the forward computation for given values of R_m, C_m and R_i; and τ_0, R_N, and C_0 are the experimentally derived values for these parameters. The N-R method iteratively computes the change required in the vector of independent variables (R_m, C_m, and R_i in the present case) to bring $f_{1,2,3,\ldots}$ closer to 0. After each iteration, the independent variables are updated; these updated values then are used in the forward computation to compute new values for the dependent variables ($\widehat{\tau_0}$, $\widehat{C_0}$, and $\widehat{R_N}$ in the present case). This process continues until there is convergence to a solu-

TABLE B1. *Spatial distribution of dendritic spines on apical and basal dendrites of model cell*

	Distance From Cell Body, μm	Density, no./μm^2 of membrane
Apical	0–25	0
	25–75	0.2
	75–100	0.5
	>100	0.8
Basal	0–10	0
	10–25	0.2
	25–50	0.5
	>50	0.8

tion (Σ_{f_i} can be made arbitrarily small) or there is no further progress toward a solution (updates to independent parameters are arbitrarily small).

APPENDIX B

Estimation of true R_m and C_m by inclusion of spine membrane

The computation of cable parameters using compartmental models that do not include dendritic spines results in an underestimation of R_m and an overestimation of C_m compared with their actual values for neuronal membrane. Assuming that spines are isopotential with dendritic shafts (Jack et al. 1975; Rapp et al. 1992; Segev and Rall 1988) and uniformly distributed, the extent of change in R_m and C_m required to compensate for the lesser membrane area when they are omitted can be estimated (see Rall et al. 1992). From estimates of spine density per unit membrane area (Table B1) and surface areas of dendritic segments, it was concluded that there were 9,089 spines on apical dendrites and 3,493 spines on basal dendrites of *cell 40C2*. From the average membrane area for spines (Table B2), it was concluded that total spine area on *40C2* was 7,849 vs. 19,409 μm^2 for dendritic shaft membrane or 29% of the total dendritic surface. This gives estimated true values of 19,725 Ωcm^2 for R_m (41% greater than without spines) and 1.06 μF/cm^2 for C_m (29% less than without spines).

APPENDIX C

Sensitivity of computed values of R_i on physiological measurements

Examination of the relationship between experimentally derived parameters (R_N, C_0, τ_0) and cable parameters (R_m, C_m, and R_i) using *cell 40C2*, revealed a source of the large range in estimates of R_i (Fig. C1). Note that C_0 (coefficient of the membrane time constant) is determined almost exclusively by R_m (Fig. C1*B*). Therefore, when R_N (input resistance) is altered at constant C_0, R_m does not change. Instead, R_i must change disproportionately to account for a small shift in R_N (because R_N is only weakly dependent on R_i, Fig. C1*A*).

When C_0 is altered at constant R_N, R_m follows (Fig. C1*B*), causing a nearly proportional change in R_N (Fig. C1*A*). Therefore, for R_N to remain constant, R_i must again change by a disproportionate amount. Thus small errors in measurement of R_N or C_0 result in a wide spread in estimates of R_i.

Nitzan et al. (1990) made the equivalent observation in simulations of vagal motoneurons, showing that at constant R_N a 10-fold change in R_i was required to account for an ~25% alteration in R_m. To obtain more accurate estimates for R_i, one would have to use physiological measures that are more sensitive to this parameter.

TABLE B2. *Dimensions of dendritic spines on model cell*

Mean head diameter	0.29 μm
Mean neck diameter	0.15 μm
Mean neck length	0.7 μm
Mean surface area (head + neck)	0.6 μm^2

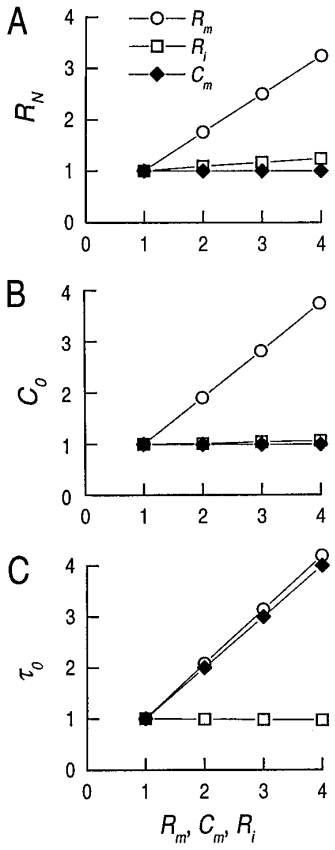

FIG. C1. Sensitivity of physiologically determined parameters (R_N, C_0, and τ_0) to values of cable parameters (R_m, C_m, and R_i). Cable parameters were varied individually, and physiological parameters determined from simulated responses to a current pulse injected into the soma of cell 40C2. *A*: input resistance, R_N, is sensitive to changes in R_m, relatively insensitive to changes in R_i, and not related to C_m. *B*: coefficient of the membrane time constant, C_0, is sensitive only to R_m. *C*: membrane time constant, τ_0, is a function of R_m and C_m, but not related to R_i.

We thank M. Hines for technical assistance with Neuron.

This work was supported by National Institute of Neurological Disorders and Stroke Grant NS-19865 to L. B. Haberly.

Present address of A. Kapur: Division of Neuroscience, Baylor College of Medicine, Houston, TX 77030.

Address for reprint requests: L. B. Haberly, Dept. of Anatomy, University of Wisconsin, 1300 University Ave., Madison, WI 53706.

Received 19 March 1997; accepted in final form 3 July 1997.

REFERENCES

ADAMS, J. C. Technical considerations on the use of horseradish peroxidase as neuronal marker. *Neuroscience* 2: 141–145, 1977.

ADAMS, J. C. Heavy metal intensification of DAB-based reaction product. *J. Histochem. Cytochem.* 29: 7751981.

ADRIAN, E. D. Olfactory reactions in the brain of the hedgehog. *J. Physiol. (Lond.)* 100: 459–473, 1942.

AIGNER, T. G. Pharmacology of memory: cholinergic-glutamatergic interactions. *Curr. Opin. Neurobiol.* 5: 155–160, 1995.

ARTOLA, A., BROCHER, S., AND SINGER, W. Different voltage-dependent thresholds for inducing long-term depression and long-term potentiation in slices of rat visual cortex. *Nature* 347: 69–72, 1990.

BARRIONUEVO, G. AND BROWN, T. H. Associative long-term potentiation in hippocampal slices. *Proc. Nat. Acad. Sci. USA* 80: 7347–7351, 1983.

BLANTON, M. G., LO TURCO, J. J., AND KRIEGSTEIN, A. R. Whole cell recording from neurons in slices of reptilian and mammalian cerebral cortex. *J. Neurosci. Methods* 30: 203–210, 1989.

DALMAZ, C., INTROINI-COLLISON, I. B., AND MCGRAUGH, J. L. Noradrenergic and cholinergic interactions in the amygdala and the modulation of memory storage. *Behav. Brain Res.* 1–2: 167–174, 1993.

DEL CERRO, S., JUNG, M., AND LYNCH, G. Benzodiazepines block long-term potentiation in slices of hippocampus and piriform cortex. *Neuroscience* 49: 1–6, 1992.

DINGLEDINE, R., HYNES, M. A., AND KING, G. L. Involvement of *N*-methyl-D-aspartate receptors in epileptiform bursting in the rat hippocampal slice. *J. Physiol. (Lond.)* 380: 175–189, 1986.

FETTIPLACE, R., ANDREWS, D. M., AND HAYDON, D. A. The thickness, composition and structure of some lipid bilayers and natural membranes. *J. Membr. Biol.* 5: 277–296, 1971.

FREUND, T. F. AND BUZAKI, G. Interneurons of the hippocampus. *Hippocampus* 6: 347–470, 1996.

GAMBLE, E. AND KOCH, C. The dynamics of free calcium in dendritic spines in response to repetitive synaptic input. *Science* 236: 1331–1335, 1987.

GARTHWAITE, G. AND GARTHWAITE, J. Quisqualate neurotoxicity: a delayed, CNQX-sensitive process triggered by a CNQX-insensitive mechanism in young rat hippocampal slices. *Neurosci. Lett.* 99: 113–118, 1989.

GILLESSEN, T. AND ALZHEIMER, C. Amplification of EPSPs by low Ni^{2+} and amiloride-sensitive Ca^{2+} channels in apical dendrites of rat CA1 pyramidal neurons. *J. Neurophysiol.* 77: 1639–1643, 1997.

GUSTAFSSON, B. AND WIGSTROM, H. Hippocampal long-lasting potentiation produced by pairing single volleys and brief conditioning tetani evoked in separate afferents. *J. Neurosci.* 6: 1575–1582, 1986.

HABERLY, L. B. Olfactory cortex. In: *Synaptic Organization of the Brain* (4th ed.), edited by G. M. Shepherd. London: Oxford, 1997.

HASSELMO, M. E. Neuromodulation and cortical function: modeling the physiological basis of behavior. *Behav. Brain Res.* 67: 1–27, 1995.

HAYDON, D. A., REQUENA, J., AND URBAN, B. W. Some effects of aliphatic hydrocarbons on the electrical capacity and ionic currents of the squid giant axon membrane. *J. Physiol. (Lond.)* 309: 229–245, 1980.

HESTRIN, S., NICOLL, R. A., PERKEL, D. J., AND SAH, P. Analysis of excitatory synaptic action in pyramidal cells using whole-cell recording from rat hippocampal slices. *J. Physiol. (Lond.)* 422: 203–225, 1990.

HINES, M. A program for simulation of nerve equations with branching geometries. *Int. J. Biomed. Comput.* 24: 55–68, 1989.

HOLMES, W. R. AND LEVY, W. B. Insights into associative long-term potentiation from computational models of NMDA receptor-mediated calcium influx and intracellular calcium concentration changes. *J. Neurophysiol.* 63: 1148–1168, 1990.

HOLMES, W. R. AND RALL, W. Estimating the electrotonic structure of neurons with compartmental models. *J. Neurophysiol.* 68: 1438–1452, 1992.

JACK, J.J.B., NOBLE, D., AND TSIEN, R. W. *Electrical Current Flow in Excitable Cells.* Oxford: Oxford 1975.

JAFFE, D. B., ROSS, W. N., LISMAN, J. E., LASSER-ROSS, N., MIYAKAWA, H., AND JOHNSTON, D. A model for dendritic Ca^{2+} accumulation in hippocampal pyramidal neurons based on fluorescence imaging measurements. *J. Neurophysiol.* 71: 1065–1077, 1994.

JAHR, C. E. AND STEVENS, C. F. A quantitative description of NMDA receptor-channel kinetic behavior. *J. Neurosci.* 10: 1830–1837, 1990a.

JAHR, C. E. AND STEVENS, C. F. Voltage dependence of NMDA-activated macroscopic conductances predicted by single-channel kinetics. *J. Neurosci.* 10: 3178–3182, 1990b.

JONAS, P., MAJOR, G., AND SAKMANN, B. Quantal components of unitary EPSCs at the mossy fibre synapse on CA3 pyramidal cells of rat hippocampus. *J. Physiol. (Lond.)* 472: 615–663, 1993.

JUNG, M. W. AND LARSON, J. Further characteristics of long-term potentiation in piriform cortex. *Synapse* 18: 298–306, 1994.

KANTER, E. D. AND HABERLY, L. B. Associative long-term potentiation in piriform cortex slices requires $GABA_A$ blockade. *J. Neurosci.* 13: 2477–2482, 1993.

KANTER, E. D., KAPUR, A., AND HABERLY, L. B. A dendritic $GABA_A$-mediated IPSP regulates facilitation of NMDA-mediated responses to burst stimulation in piriform cortex. *J. Neurosci.* 16: 307–312, 1996.

KAPUR, A., PEARCE, R. A., AND HABERLY, L. B. $GABA_A$ -mediated IPSCs in piriform cortex have fast and slow components with different properties and locations on pyramidal cells. *J. Neurophysiol.* 78: 2531–2545, 1997.

KETCHUM, K. L. AND HABERLY, L. B. Synaptic events that generate fast oscillations in piriform cortex. *J. Neurosci.* 13: 3980–3985, 1993a.

KETCHUM, K. L. AND HABERLY, L. B. Membrane currents evoked by afferent fiber stimulation in rat piriform cortex. II. Analysis with a system model. *J. Neurophysiol.* 69: 261–281, 1993b.

LEVY, W. B. AND STEWARD, O. Synapses as associative memory elements in the hippocampal formation. *Brain Res.* 175: 233–245, 1979.

LIPOWSKY, R., GILLESSEN, T., AND ALZHEIMER, C. Dendritic Na^+ channels amplify EPSPs in hippocampal CA1 pyramidal cells. *J. Neurophysiol.* 76: 2181–2191, 1996.

LUHMANN, H. J. AND PRINCE, D. A. Control of NMDA receptor-mediated activity by GABAergic mechanisms in mature and developing rat neocortex. *Dev. Brain Res.* 54: 287–290, 1990.

MAGEE, J. C. AND JOHNSTON, D. Characterization of single voltage-gated Na^+ and Ca^{2+} channels in apical dendrites of rat CA1 pyramidal neurons. *J. Physiol. (Lond.)* 487: 67–90, 1995.

MAGEE, J. C. AND JOHNSTON, D. A synaptically controlled, associative signal for Hebbian plasticity in hippocampal neurons. *Science* 275: 209–213, 1997.

MAJOR, G., LARKMAN, A. U., JONAS, P., SAKMANN, B., AND JACK, J.J.B. Detailed passive cable models of whole-cell recorded CA3 pyramidal neurons in rat hippocampal slices. *J. Neurosci.* 14: 4613–4638, 1994.

MARKRAM, H., LUBKE, J., FROTSCHER, M., AND SAKMANN, B. Regulation of synaptic efficacy by coincidence of postsynaptic APs and EPSPs. *Science* 275: 213–215, 1997.

MILES, R., TÓTH, K. GULYÁS, A. I., HÁJOS, N. AND FREUND, T. F. Differences between somatic and dendritic inhibition in the hippocampus. *Neuron* 16: 815–823, 1996.

NABESHINA, T. Behavioral aspects of cholinergic transmission: role of basal forebrain cholinergic system in learning and memory. *Prog. Brain Res.* 98: 405–411, 1993.

NEVEU, D. AND ZUCKER, R. S. Postsynaptic levels of $[Ca^{2+}]_i$ needed to trigger LTD and LTP. *Neuron* 16: 619–629, 1996.

NITZAN, R., SEGEV, I., AND YAROM, Y. Voltage behavior along the irregular dendritic structure of morphologically and physiologically characterized vagal motoneurons in the guinea pig. *J. Neurophysiol.* 63: 333–346, 1990.

PEARCE, R. A. Physiological evidence for two distinct $GABA_A$ responses in rat hippocampus. *Neuron* 10: 189–200, 1993.

PERKEL, D. H., MULLONEY, B., AND BUDELLI, R. W. Quantitative methods for predicting neuronal behavior. *Neuroscience* 6: 823–837, 1981.

PEROUANSKY, M. AND YAARI, Y. Kinetic properties of NMDA receptor-mediated synaptic currents in rat hippocampal pyramidal cells versus interneurones. *J. Physiol. (Lond.)* 465: 223–244, 1993.

PRESS, W. H., TEUKOLSKY, S. A., VETTERLING, W. T., AND FLANNERY, B. P. *Numerical Recipes in C: The Art of Scientific Computing.* Cambridge, UK: Cambridge Univ. Press, 1992.

RALL, W., BURKE, R. E., HOLMES, W. R., JACK, J.J.B., REDMAN, S. J., AND SEGEV, I. Matching dendritic neuron models to experimental data. *Physiol. Rev.* 72: S159–S186, 1992.

RAPP, M., YAROM, Y., AND SEGEV, I. The impact of parallel fiber background activity on the cable properties of cerebellar Purkinje cells. *Neural Comput.* 4: 518–533, 1992.

SARA, S. J., VANKOV, A., AND HERVE, A. Locus coeruleus-evoked responses in behaving rats: a clue to the role of noradrenaline in memory. *Brain Res. Bull.* 5–6: 457–465, 1994.

SCHOLFIELD, C. N. A depolarizing inhibitory potential in neurones of the olfactory cortex in vitro. *J. Physiol. (Lond.)* 275: 547–557, 1978.

SCHWINDT, P. C. AND CRILL, W. E. Amplification of synaptic current by persistent sodium conductance in apical dendrite of neocortical neurons. *J. Neurophysiol.* 74: 2220–2224, 1995.

SEGEV, I. AND RALL, W. Computational study of an excitable dendritic spine. *J. Neurophysiol.* 60: 499–523, 1988.

SPRUSTON, N. AND JOHNSTON, D. Perforated patch-clamp analysis of the passive membrane properties of three classes of hippocampal neurons. *J. Neurophysiol.* 67: 508–529, 1992.

STECKLER, T. AND SAHGAL, A. The role of serotonergic-cholinergic interactions in the mediation of cognitive behavior. *Behav. Brain Res.* 67: 165–199, 1995.

STERN, P., EDWARDS, F. A., AND SAKMANN, B. Fast and slow components of unitary EPSCs on stellate cells elicited by focal stimulation in slices of rat visual cortex. *J. Physiol. (Lond.)* 449: 247–278, 1992.

STEWARD, O., TOMASULO, R., AND LEVY, W. B. Blockade of inhibition in a pathway with dual excitatory and inhibitory action unmasks a capability for LTP that is otherwise not expressed. *Brain Res.* 516: 292–300, 1990.

SVOBODA, K., DENK, W., KLEINFELD, D., AND TANK, D. W. In vivo dendritic calcium dynamics in neocortical pyramidal neurons. *Nature* 385: 161–165, 1997.

TAKASHIMA, S. Membrane capacity of squid giant axon during hyper- and depolarizations. *J. Membr. Biol.* 27: 21–39, 1976.

THURBON, D., FIELD, A., AND REDMAN, S. J. Electrotonic profiles of interneurons in stratum pyramidale of the CA1 region of the rat hippocampus. *J. Neurophysiol.* 71: 1948–1958, 1994.

TOMASULO, R. A., RAMIREZ, J. J., AND STEWARD, O. Synaptic inhibition regulates associative interactions between afferents during the induction of long-term potentiation and depression. *Proc. Nat. Acad. Sci. USA* 90: 11578–11582, 1993.

TSENG, G.-F. AND HABERLY, L. B. Characterization of synaptically mediated fast and slow inhibitory processes in piriform cortex in an in vitro slice preparation. *J. Neurophysiol.* 59: 1352–1376, 1988.

TURNER, D. A. Segmental cable evaluation of somatic transients in hippocampal neurons (CA1, CA3, and dentate). *Biophys. J.* 46: 73–84, 1984.

ZADOR, A., KOCH, C., AND BROWN, T. H. Biophysical model of a Hebbian synapse. *Proc. Nat. Acad. Sci. USA* 87: 6718–6722, 1990.

ZHANG, D. X. AND LEVY, W. B. Bicuculline permits the induction of long-term depression by heterosynaptic, translaminar conditioning in the hippocampal dentate gyrus. *Brain Res.* 613: 309–312, 1993.